



Semiclassical thermodynamic geometry

L. F. Escamilla-Herrera ^{*}, J. L. López-Picón [†], José Torres-Arenas [‡], and Alejandro Gil-Villegas [§]
División de Ciencias e Ingenierías Campus León, Universidad de Guanajuato, AP E-143, CP 37150, León, Guanajuato, México

 (Received 10 January 2024; revised 12 March 2024; accepted 23 May 2024; published 20 June 2024)

In this work the thermodynamic geometry (TG) of semiclassical fluids is analyzed. We present results for two models. The first one is a semiclassical hard-sphere (SCHS) fluid whose Helmholtz free energy is obtained from path-integral Monte Carlo simulations. It is found that, due to quantum contributions in the thermodynamic potential, the anomaly found in TG for the classical hard-sphere fluid related to the sign of the scalar curvature is now avoided in a considerable region of the thermodynamic space. The second model is a semiclassical square-well fluid, described by a SCHS repulsive interaction coupled with a classical attractive square-well contribution. The behavior of the semiclassical curvature scalar as a function of the thermal de Broglie wavelength λ_B is analyzed for several attractive-potential ranges. A description of the semiclassical R Widom lines, defined by the maxima of the curvature scalar, is also obtained and results are compared with the corresponding classical systems for different square-well ranges.

DOI: [10.1103/PhysRevE.109.064145](https://doi.org/10.1103/PhysRevE.109.064145)

I. INTRODUCTION

Semiclassical fluids (SCFs) are an important subject within the molecular liquids research community. Unlike classical fluids, in the quantum regime the dual wave-particle nature of the individual constituents becomes dominant and manifests in their collective properties. These systems defy our classical understanding of matter and offer exciting prospects for technological advancements, considering substances like hydrogen and helium, and their transport and storage. Additionally, quantum properties of the hydrogen bond have been of increasing interest recently [1] as well as their significance in the description of the phase diagram of associating fluids [2]. On the other hand, research on SCFs gives insight into the fundamental principles of quantum mechanics, shedding light on the nature of matter and its interactions under extreme conditions. In this paper we explore some aspects of the thermodynamic properties of SCFs using the thermodynamic geometry formalism, highlighting the main aspects such as the Riemann scalar curvature and the R Widom line.

Semiclassical hard-sphere (SCHS) fluid is a natural system to study since it is possible to compare quantum effects with respect to the very-well-known classical hard-sphere (HS) system. Analytical results are known for the Slater sum of SCHS fluids at low densities, obtaining interesting insights into quantum effects in semiclassical computer simulation studies [3]. Thermodynamic, structural, and dynamic properties of SCHS fluids have been studied using the more robust path-integral Monte Carlo (PIMC) method [4–6] for a wide range of densities ρ , temperatures T , and thermal de Broglie

wavelength values λ_B and for a system of particles at temperature T , with $\lambda_B = h/\sqrt{2\pi mkT}$, where m is the mass per particle and h and k are the Planck and Boltzmann constants, respectively. In order to consider attractive interactions for a more realistic description of real fluid systems, different hard-core potential equations of state have been developed, such as for semiclassical square-well [7,8] and semiclassical Yukawa [9] fluids.

The simulation method used to obtain a semiclassical equation of state, as described by Serna and Gil-Villegas [8], is based on the isomorphism between Feynman's path integrals and the statistical mechanics of classical ring molecules, since a quantum propagator is transformed into a partition function using a complex time $\tau = ih/kT$ according to the Wick transformation [10–12]. Since exchange effects provide a very small contribution to the statistical properties, as has been shown by Singer and Smith [13] and Runge and Chester [4], the isomorphism uses a Boltzmann-Gibbs statistics. The equation of state used in this work, described in Ref. [8], was obtained from a reparametrization of the Carnahan-Starling equation of state for classical hard spheres, using an effective packing fraction dependent on the actual value of the packing fraction and λ_B , in order to reproduce PIMC results. The PIMC simulations were obtained in the NVT ensemble for 125 necklaces and 6 beads per ring molecule, using 1.28×10^5 and 1.28×10^6 bead cycles for equilibration and for averaging, respectively. The quantization method is useful to describe bulk and confined phases of hydrogen, deuterium, and helium-4, as we have previously reported [14]. Low temperatures are not necessarily required when confinement is present, since diffraction effects are also relevant when λ_B is comparable to the size of pores, as has been determined in adsorption of hydrogen in polymeric networks (see, e.g., the work of Arriola-González *et al.* [15]).

In the past few decades, several approaches have been developed to describe thermodynamic properties of systems

^{*}Contact author: lescamilla@fisica.ugto.mx

[†]Contact author: jl_lopez@fisica.ugto.mx

[‡]Contact author: jtorres@fisica.ugto.mx

[§]Contact author: gil@fisica.ugto.mx

using differential geometry. Most of these theories are consequences of the well-known fluctuation theory [16–18], establishing the notion of distance between a pair of points, each one representing a thermodynamic state, located on the space composed of thermodynamic parameters. In the context of Riemannian geometry, such a distance plays the role of the metric. In particular, Weinhold [19] and Ruppeiner [20,21] defined Hessian metrics in terms of a given thermodynamic potential in the thermodynamic equilibrium space, the internal energy (Weinhold), and the entropy (Ruppeiner). In Ruppeiner's work, its metric is the negative of the Hessian of the entropy. Both metrics are related by a conformal factor [22]. The theoretical framework of such Hessian metrics is usually referred to in the literature as thermodynamic geometry (TG). This formalism is considered in the present work to study the physical properties of the SCHS and semiclassical square-well (SSW) fluids.

In this work we are also interested in the study of the SCF supercritical region using the TG approach. This region is of great interest for both theoretical and experimental research, particularly the estimation of the existing boundary which separates the gaslike and liquidlike phases, which has been observed in the supercritical region [23–25]. One of these boundaries is the so-called Widom line [24,26,27], which is defined as the locus of points that maximize the correlation length. It is known that the correlation length diverges at the critical point, but above its vicinity changes with a defined power law [23]. This behavior makes it possible to characterize this curve through extreme values of the correlation length and near the critical point, via the extreme values of different response functions. It is well known that such curves exhibit a linear behavior in the region close to the critical point, to later separate from each other as temperature increases. Therefore, the coincidence of such lines in the (P, T) plane has been used previously as a definition for a unique Widom line [24,28,29].

A more recent proposal to define the Widom line comes from the TG framework, which defines this curve as the locus of maxima of the isotherms of the scalar curvature obtained for the thermodynamic metric constructed using this formalism [30,31]; this is known as the R Widom line. It is important to stress that, at present, there is no consensus on a single definition of the Widom line. Some of the most common definitions in the literature involve the maxima of certain response functions (heat capacities, compressibilities, etc.). Another definition, as previously mentioned, refers to the Widom line as the maxima of the correlation length. Since we are working within a TG formalism, in this work the R Widom line definition will be used to explore the supercritical behavior of the SSW fluid.

This work is organized as follows. In Sec. II we briefly present how the metric and curvature are calculated in terms of the dimensionless Helmholtz free-energy representation. Subsequently, equations of state related to the classical and semiclassical HS systems are presented together with the geometrical analysis of their curvatures, as well as a discussion about its consequences. Section III presents the TG analysis for the SSW fluid and the Widom lines for different values of the square-well (SW) range λ . Finally, a summary and prospective avenues of research are given in Sec. IV.

II. THERMODYNAMIC GEOMETRY: CLASSICAL AND SEMICLASSICAL HARD-SPHERE FLUID

In this section we will consider the TG formalism [20,21] for a SCHS fluid. We use the Helmholtz free-energy representation for which the thermodynamic metric components are obtained as second derivatives of the free energy per volume $f = A/V$ with respect to absolute temperature T and number density $\rho = N/V$. This metric is given in its matrix form by

$$[g_{ij}] = \frac{1}{kT} \begin{pmatrix} -\frac{\partial^2 f}{\partial T^2} & 0 \\ 0 & \frac{\partial^2 f}{\partial \rho^2} \end{pmatrix}. \quad (1)$$

In the statistical associating fluid theory (SAFT) approach, developed for chain molecules of hard-core segments with attractive potentials of variable range (SAFT-VR) [32,33], which will be followed in subsequent sections, the dimensionless free energy is defined by

$$\frac{A}{NkT} = a(T, \rho). \quad (2)$$

The TG metric components of the system are determined by

$$\begin{aligned} g_{TT} &= \frac{6}{\pi\sigma^3} \left(\frac{2\eta}{T} \frac{\partial a}{\partial T} - \frac{\partial^2 a}{\partial T^2} \right), \\ g_{\eta\eta} &= \frac{\pi\sigma^3}{6} \left(\eta \frac{\partial^2 a}{\partial \eta^2} + 2 \frac{\partial a}{\partial \eta} \right), \end{aligned} \quad (3)$$

where η is the packing fraction for hard-sphere particles with diameter σ , obtained from the density number as

$$\eta = \pi\rho\sigma^3/6. \quad (4)$$

The corresponding reduced curvature scalar $R^* = R/\sigma^3$ is given by

$$R^* = \frac{\pi^2\sigma^3}{36\sqrt{g}} \frac{\partial}{\partial \eta} \left(\frac{1}{\sqrt{g}} \frac{\partial g_{TT}}{\partial \eta} \right) - \frac{1}{\sigma^3\sqrt{g}} \frac{\partial}{\partial T} \left(\frac{1}{\sqrt{g}} \frac{\partial g_{\eta\eta}}{\partial T} \right). \quad (5)$$

This form of R^* is particularly simple because the metric is diagonal in the Helmholtz free-energy representation [20,30]. According to the TG approach and following the sign convention in [21], negative (positive) values for R indicate that attractive (repulsive) interactions are predominant in the system under study. However, it is well known that the TG description for a classical HS fluid presents a fundamental inconsistency related to the interpretation of the sign of R (see, for instance, Ref. [30]), since the corresponding scalar curvature, calculated for different equations of state, is always negative, which contradicts the repulsive nature of the hard-sphere potential. This convention will also be followed here. Furthermore, for semiclassical system results it is convenient to represent the curvature in terms of λ_B instead of temperature. This change results in a global minus sign that reverses the sign interpretation of R .

In the fluid region of the phase diagram of a classical hard-sphere fluid, the Helmholtz free energy can be accurately described by the Carnahan-Starling equation [34]

$$\frac{A_{HS}}{NkT} = \ln(\rho\lambda_B^3) - 1 + \frac{4\eta - 3\eta^2}{(1 - \eta)^2}. \quad (6)$$

The TG applied to the classical HS fluid was partially analyzed in Ref. [35], where the curvature R of the free energy (6) was computed and compared with values determined with another HS model [30]. It was observed for both models that the interaction hypothesis related to the thermodynamic curvature of the HS system was not valid, since the HS curvature always remains negative. Given the fact that there is no attractive contribution to the HS interaction, the sign of its curvature contradicts the aforementioned hypothesis. This is known in the literature as the Brańka-Pieprzyk-Heyes (BPH) anomaly [36]. In what follows, a model of a SCHS fluid will be analyzed with the premise that the BPH anomaly could be solved when quantum contributions are taken into account.

Quantum corrections to classical equations of state (EOSs) can be introduced according to semiclassical thermodynamic perturbation methods [2,8]. These EOSs are given as functions of λ_B . In [8] the functional expression of the Carnahan-Starling excess Helmholtz free energy was used to obtain a parametrization valid for a SCHS fluid in order to reproduce PIMC simulation values. The corresponding SCHS Helmholtz free energy can be expressed in terms of an effective packing fraction η_e ,

$$\frac{A^{\text{SCHS}}}{NkT} = \frac{4\eta_e - 3\eta_e^2}{(1 - \eta_e)^2}, \quad (7)$$

where η_e is a function of the actual packing fraction η and the reduced de Broglie thermal wavelength $\lambda_B^* = \lambda_B/\sigma$,

$$\eta_e = (1 + d_1\lambda_B^*)\eta + (d_2\lambda_B^* + d_3\lambda_B^{*2})\eta^2, \quad (8)$$

with $d_1 = 1.659\,385\,448\,4$, $d_2 = -1.092\,711\,515\,0$, and $d_3 = -1.118\,823\,392\,1$.

For the purpose of exploring geometric properties of Eq. (7) it is convenient to construct the TG formulation in terms of λ_B instead of the usual variable temperature T . In order to do this, it is useful to introduce the reduced temperature $T^* = kT/\epsilon$, where the energy parameter ϵ is related to the potential depth of a particular attractive interaction. Although this not apply for the HS system, it is possible to define a suitable energy parameter, denoted by ϵ_0 , given by

$$\epsilon_0 = \frac{h^2}{2\pi m\sigma^2}, \quad (9)$$

and then $T_{\text{HS}}^* = kT/\epsilon_0$.

The reduced thermal wavelength λ_B^* is given in terms of the de Boer parameter $\Lambda = h/\sigma\sqrt{m\epsilon}$ as

$$\lambda_B^* = \frac{\Lambda}{\sqrt{2\pi}\sqrt{T^*}}, \quad T^* = \frac{kT}{\epsilon}. \quad (10)$$

For the SCHS system the corresponding expression is

$$\lambda_B^* = \frac{\Lambda_0}{\sqrt{2\pi}\sqrt{T_{\text{HS}}^*}} = \frac{1}{\sqrt{T_{\text{HS}}^*}}, \quad (11)$$

where $\Lambda_0 = \sqrt{2\pi}$, which is very close to the de Boer parameter for atomic hydrogen. This procedure for Λ will also be used to obtain the geometric properties of the SSW systems since it allows us to write the geometric properties of the HS system in terms of the reduced thermal wavelength λ_B^* by using the relation $\lambda_B^* = 1/\sqrt{T_{\text{HS}}^*}$.

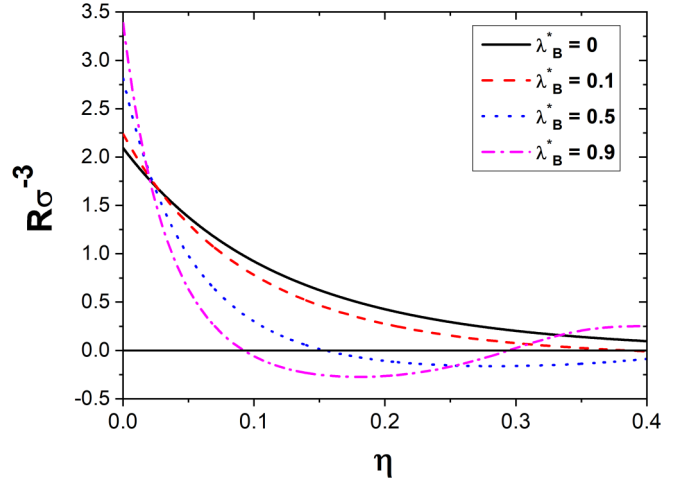


FIG. 1. Reduced curvature for the classical and semiclassical hard-sphere systems for different isotherms in the (λ_B^*, η) representation. The solid line for $\lambda_B^* \rightarrow 0$ represents the behavior for a classical HS fluid; as λ_B^* increases (temperature decreases), the quantum contribution becomes more important in the region where the curvature becomes negative, crossing the $R^* = 0$ line, reversing the known anomaly for the classical HS curvature.

The geometric properties of the SCHS system can be rewritten in terms of derivatives with respect to λ_B^* using Eq. (11),

$$g_{\lambda_B^* \lambda_B^*} = -\frac{3\eta}{2\pi\sigma^3} \left(\lambda_B^{*2} \frac{\partial^2 a}{\partial \lambda_B^{*2}} - \lambda_B^{*5} \frac{\partial a}{\partial \lambda_B^*} \right), \quad (12a)$$

$$g_{\eta\eta} = \frac{\pi\sigma^3}{6} \left(\eta \frac{\partial a^2}{\partial \eta^2} + 2 \frac{\partial a}{\partial \eta} \right), \quad (12b)$$

and hence the curvature scalar is given by

$$R^* = \frac{\pi^2\sigma^3}{36\sqrt{g}} \frac{\partial}{\partial \eta} \left(\frac{1}{\sqrt{g}} \frac{\partial g_{\lambda_B^* \lambda_B^*}}{\partial \eta} \right) - \frac{\lambda_B^{*3}}{4\sigma^3\sqrt{g}} \frac{\partial}{\partial \lambda_B^*} \left(\frac{\lambda_B^{*3}}{\sqrt{g}} \frac{\partial g_{\eta\eta}}{\partial \lambda_B^*} \right). \quad (13)$$

As long as the free-energy representation is used, the curvature R^* given in (13) remains the same, regardless of the particular model; therefore, it will be used to calculate R^* for the classical and semiclassical SW fluids described in the next section.

The results for R^* for the SCHS system are presented in Fig. 1, where several isotherms in the (λ_B^*, η) representation are plotted. The solid line represents the classical case, which corresponds to the isotherm where $\lambda_B^* \rightarrow 0$, for which, in the range of validity for the EOS given by (7), R^* is always positive, i.e., negative in the T - η thermodynamic space. As λ_B^* increases, quantum effects become more noticeable, since a change in the sign of the curvature appears at small densities. In such a region, the usual interpretation given in the literature of the sign of R^* is then fulfilled. However, for even greater values of λ_B^* , another change of sign appears, returning to the BPH anomaly for R^* in the region of higher values of η , therefore constraining the region where quantum effects are able to reverse this anomaly. For instance, in the isotherm $\lambda_B^* = 0.9$ (dash-dotted line) a bump underneath the line $R^* = 0$ is observed; this is the region for which the usual TG interpretation of a repulsive interaction holds.

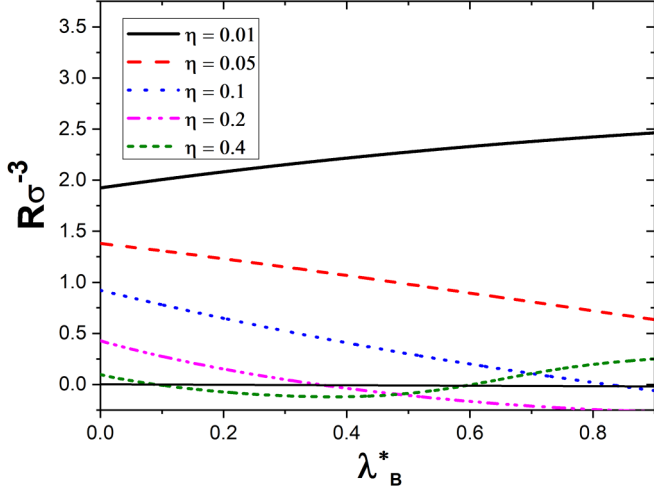


FIG. 2. Reduced curvature for the SCHS system in the (λ_B^*, η) representation for different values of η . The crossing through zero of the semiclassical curvature is also favored by increasing density. This behavior for both λ_B^* and η is better depicted in the three-dimensional representation of R^* .

This interpretation is reinforced in Fig. 2, where R^* is given in the (λ_B^*, η) representation for several values of the packing fraction. A change of sign appears in R^* starting from the curve $\eta = 0.1$. The bump region where the BPH anomaly is reversed can also be noticed in this figure, appearing at higher densities; it is clearly visible from $\eta = 0.2$ and around the interval $0.1 \leq \lambda_B^* \leq 0.6$.

In order to better depict the behavior of the curvature of the semiclassical SCHS system, a three-dimensional (3D) plot in the (λ_B^*, η) representation is presented in Fig. 3. This plot also presents the plane of flat curvature $R^* = 0$. The region below this plane with negative curvature, as observed in Fig. 1, becomes a strip that crosses the middle section of the plot. This is the region where quantum effects reverse the BPH anomaly in the curvature of the SCHS system, since in the usual (T, η) representation, curvature becomes positive now,

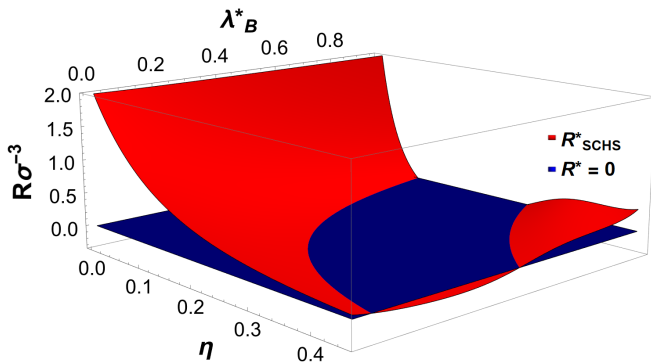


FIG. 3. Plot of the 3D reduced curvature scalar R_{SCHS}^* for the SCHS system as a function of λ_B^* and η . The crossing with the $R^* = 0$ plane is also presented. The main feature of this plot is the existence of a region of (λ_B^*, η) for which the interpretation of the sign of the curvature scalar holds, located in the strip around the middle section of η .

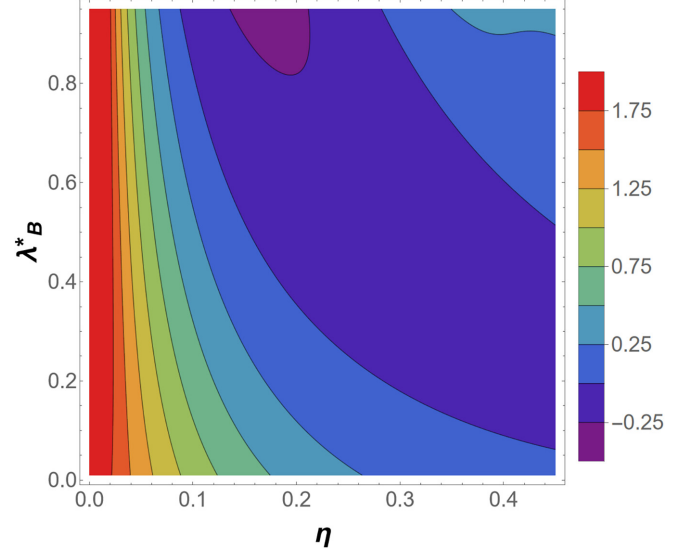


FIG. 4. Contour plot for the curvature scalar for the SCHS system in the (λ_B^*, η) space. The region where $R^* < 0$ (i.e., where the BPH anomaly is reversed) is located in the strip in the middle of the plot limited by the lower and upper contour lines, whereas for high values of λ_B^* and η the value of R^* becomes positive once again. A region of minimum values for the curvature also appears in the upper middle section of the plot.

consistent with the interpretation given in the TG literature of a repulsive potential, as is the case of the HS fluid.

Finally, a contour plot of λ_B^* vs η for the SCHS curvature R^* is presented in Fig. 4. This plot describes the values that curvature R^* takes in the (λ_B^*, η) representation. The region where the BPH anomaly is reversed due to quantum effects is also present in the middle section, enclosed by the lines where $R^* = 0$. This region is the same one observed in Fig. 3. Additionally, the existence of a small U-shaped region around $\lambda_B^* = 0.8$ and $\eta = 0.2$ can be noticed, which is the region where the lowest value [or highest value in the (T, η) representation] of the curvature is reached.

III. THERMODYNAMIC GEOMETRY OF THE SEMICLASSICAL SQUARE-WELL FLUID

In this section the TG of a semiclassical SW fluid is explored. This is achieved by coupling the SCHS equation of state (7) with a classical SW potential, a first approach to explore thermodynamic geometric properties of a semiclassical SW fluid. In this regard, the SW fluid is a more general and interesting system whose classical thermodynamics has been widely studied [37–42]. In the case of SSW systems, several models have been developed previously (see, for instance, Refs. [2,7,8]). We consider a thermodynamic perturbation approach with the SCHS contribution described in Sec. II as the reference system, given by the semiclassical Helmholtz free energy (7), coupled with the classical SW contribution presented in [43] as a perturbation,

$$\frac{A}{Nk_B T} = \frac{A^{\text{ideal}}}{Nk_B T} + \frac{A^{\text{SCHS}}}{Nk_B T} + \frac{A_1}{Nk_B T} + \frac{A_2}{Nk_B T}, \quad (14)$$

where A_1 and A_2 are the first SW perturbation terms used in the optimized SW equation of state in the SAFT-VR approach [33]. The first contribution $A_1/Nk_B T$ is given by

$$\frac{A_1}{Nk_B T} = -4 \left(\frac{\epsilon}{kT} \right) (\lambda^{*3} - 1) \eta G_{\text{HS}}(1; \eta_{\text{eff}}), \quad (15)$$

where $G^{\text{HS}}(1; \eta_{\text{eff}})$ is the contact value of the radial distribution function evaluated at an effective packing fraction η_{eff} ,

$$G_{\text{HS}}(1; \eta_{\text{eff}}) = \frac{1 - \eta_{\text{eff}}/2}{(1 - \eta_{\text{eff}})^3}. \quad (16)$$

The effective packing fraction is parametrized using a Padé approximation [33]

$$\eta_{\text{eff}} = \frac{c_1 \eta + c_2 \eta^2}{(1 + c_3 \eta)^3}, \quad (17)$$

where the indexed constants c_i ($i = 1, 2, 3$) are given in terms of the reduced SW range $\lambda^* = \lambda/\sigma$, which can be written as

$$\begin{aligned} c_1 &= -\frac{3.1649}{\lambda^*} + \frac{13.3501}{\lambda^{*2}} - \frac{14.8057}{\lambda^{*3}} + \frac{5.7029}{\lambda^{*4}}, \\ c_2 &= \frac{43.0042}{\lambda^*} - \frac{191.6623}{\lambda^{*2}} + \frac{273.8968}{\lambda^{*3}} - \frac{128.9334}{\lambda^{*4}}, \\ c_3 &= \frac{65.0419}{\lambda^*} - \frac{266.4627}{\lambda^{*2}} + \frac{361.0431}{\lambda^{*3}} - \frac{162.6996}{\lambda^{*4}}. \end{aligned} \quad (18)$$

These inverse-power expansions in λ^* ensure that $\eta_{\text{eff}} \rightarrow 0$ for $\lambda^* \rightarrow \infty$, from which the desired behavior in the mean-field limit $G_{\text{HS}}(1; \eta_{\text{eff}}) \rightarrow 1$ is recovered. The second-order fluctuation term $A_2/Nk_B T$ is computed using the local-compressibility approximation [32,33],

$$\frac{A_2}{Nk_B T} = \frac{1}{2} \left(\frac{\epsilon}{kT} \right) K^{\text{HS}} \eta \frac{\partial}{\partial \eta} \left(\frac{A_1}{Nk_B T} \right), \quad (19)$$

where K^{HS} is the HS isothermal compressibility [44]

$$K^{\text{HS}} = \frac{(1 - \eta)^4}{1 + 4\eta + 4\eta^2 - 4\eta^3 + \eta^4}. \quad (20)$$

Before proceeding to obtain the curvature of the free energy given in Eq. (14), it is important to make the following point. As mentioned before when the geometric properties of the SCHS system were derived, it is convenient to express the free energy of the semiclassical and classical SW fluids in terms of the thermal de Broglie wavelength λ_B^* , including the explicit terms depending on temperature, according to the relation $\lambda_B^* = \Lambda/\sqrt{2\pi T^*}$, with $T^* = kT/\epsilon$. In the case of the SSW system the energy parameter used to scale the temperature is ϵ , the energy depth of the square well. We use this natural scaling instead of the SCHS parameter (9). Therefore, we have two different reduced temperatures $T_{\text{SW}}^* = kT/\epsilon$ and $T_{\text{HS}}^* = kT/\epsilon_0$ for the SW and HS potentials, respectively. From the relation between the thermal de Broglie wavelength and the de Boer parameter, presented in Eq. (10), it follows that when this parameter is set equal to $\Lambda = \sqrt{2\pi}$, it basically corresponds to the atomic hydrogen value, the energy parameters ϵ and ϵ_0 are indeed equal, and the same is also true for the reduced temperatures. This allows us to write the complete free energy in terms of only one reduced temperature. In addition, the relation between λ_B^* and T^* is simply $\lambda_B^* = 1/\sqrt{T^*}$

TABLE I. Theoretical critical values in the (T^*, η) representation of the semiclassical and classical SW fluid are presented for different potential ranges between 1.25 and 3.0, denoted by η_{crit} and η_{ccrit} , respectively.

λ^*	η_{crit}	T_{crit}^*	P_{crit}^*	η_{ccrit}	T_{ccrit}^*	P_{ccrit}^*
1.25	0.0314	0.2378	0.0047	0.2239	0.83627	0.1649
1.50	0.0404	0.4932	0.0126	0.1499	1.32907	0.1434
1.75	0.0475	0.8487	0.0255	0.1232	1.9073	0.1583
2.00	0.0566	1.3782	0.0493	0.1247	2.8248	0.2325
2.50	0.0783	3.3019	0.1673	0.1330	5.8015	0.5226
3.00	0.0931	6.7089	0.4201	0.1336	10.3288	2.3393

and the change of variable applied to calculate the curvature of the SCHS system can also be applied without any further modifications. The corresponding expressions for the metric components and curvature are the same as those ones given by Eqs. (12) and (13), respectively.

The TG metric of the semiclassical SW fluid is obtained through second-order derivatives of the Helmholtz free energy given in Eq. (14) and applying Eq. (1). In order to compare how this geometric property changes by introducing the SCHS potential given in Eq. (7), the classical SW fluid model presented in [43] is used as a reference. In Table I the critical values for different potential ranges for the classical and semiclassical SW fluids are presented in the (T^*, η) representation. It can be noticed that the critical values of the semiclassical system are considerably lower when compared to the classical ones.

Once both metric elements and curvatures are calculated for the semiclassical and classical SW fluids using Eqs. (3) and (13) in the (λ_B^*, η) representation, an analysis of their behavior is performed in the supercritical region of λ_B^* , in order to avoid any singularity due to the gas-liquid phase transition. First, a 2D comparison of the curvature scalar for different isotherms is presented in Fig. 5 for a SW range $\lambda^* = 1.5$ for both semiclassical and classical systems (solid and dashed lines, respectively). Three different temperatures are considered for this comparison, namely, $T^* = 1.25T_{\text{crit}}^*$, $2.0T_{\text{crit}}^*$, and $3.0T_{\text{crit}}^*$; these particular values were chosen to fairly compare the corresponding curvatures since the critical points for each system are not close to each other, as noticed in Table I. The main remark about Fig. 5 is that the maximum of R^* reached for the semiclassical SW is higher when compared to the classical one at the same ‘‘distance’’ from their corresponding critical point. The semiclassical system has a steeper maximum and is located at smaller packing fractions compared to the classical SW fluid. This feature is more evident upon reaching the critical point of each system.

Figure 6 presents 3D plots of the semiclassical (red surface) and classical (blue surface) SW fluid for the curvature scalars in the thermodynamic space (λ_B^*, η) for a SW $\lambda^* = 1.5$. As in the case of the two-dimensional plots presented in Fig. 5, these surfaces were obtained for the supercritical region to avoid any singularity in R^* close to the critical point, starting from $0.3\lambda_{B_{\text{crit}}}^*$ up to $0.8\lambda_{B_{\text{crit}}}^*$, i.e., from 30% to 80% of the critical value in λ_B^* . From this figure it can be noticed that the curvature of the semiclassical and classical SW fluids

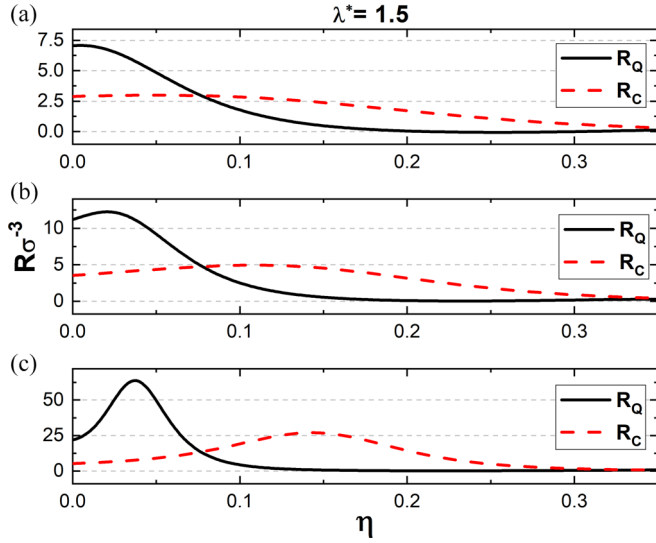


FIG. 5. Isotherms of the curvature R of the semiclassical (solid lines) and classical (dashed lines) SW fluid for a potential range of $\lambda^* = 1.5$ in the supercritical region. To gain further insight into the behavior of both systems, T^* is set equal to (a) $3T_{crit}^*$, (b) $2T_{crit}^*$, and (c) $1.25T_{crit}^*$, namely, at the same percentage away from its corresponding critical value.

greatly differs in the region $\eta \rightarrow 0$, i.e., for small densities, where quantum effects are more relevant. This behavior is also captured in the 2D plots.

In order to display the differences in the behavior between the semiclassical and classical curvature scalars of the SW fluid, the normalized difference $\Delta R = (R_Q^* - R_C^*)/R_Q^*$ of the reduced curvatures for a potential range of $\lambda^* = 1.5$ is presented in Fig. 7. In this figure, ΔR is calculated considering thermodynamic variables reduced with their corresponding critical values, i.e., $\eta^+ = \eta/\eta_{crit}$ and $T^+ = T/T_{crit}$, and using a counter i to increase the values of the thermodynamic parameters. Critical reduced values are considered to compare

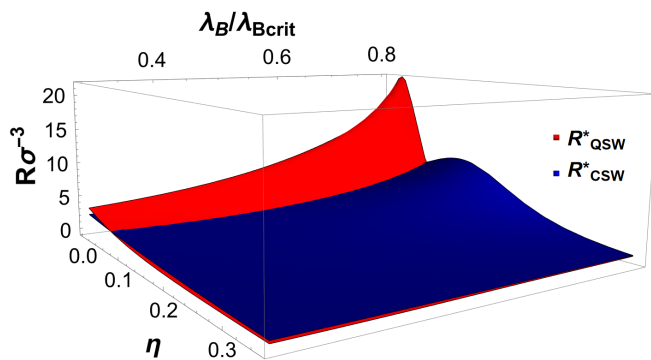


FIG. 6. 3D plot of the reduced semiclassical (R_{QSW}^*) and classical (R_{CSW}^*) SW curvatures. Both plots are determined for the same SW range, $\lambda^* = 1.5$. The corresponding thermal de Broglie wavelength values at the critical temperatures are $\lambda_B^{SC} = 1.4239$ and $\lambda_B^C = 0.8674$ for the semiclassical and classical curvatures, respectively. In order to avoid singularities due to the gas-liquid transition, the plot is constructed considering only supercritical values of λ_B^* for each system within $0.3 \leq \lambda_B^*/\lambda_{Bcrit}^* \leq 0.8$.

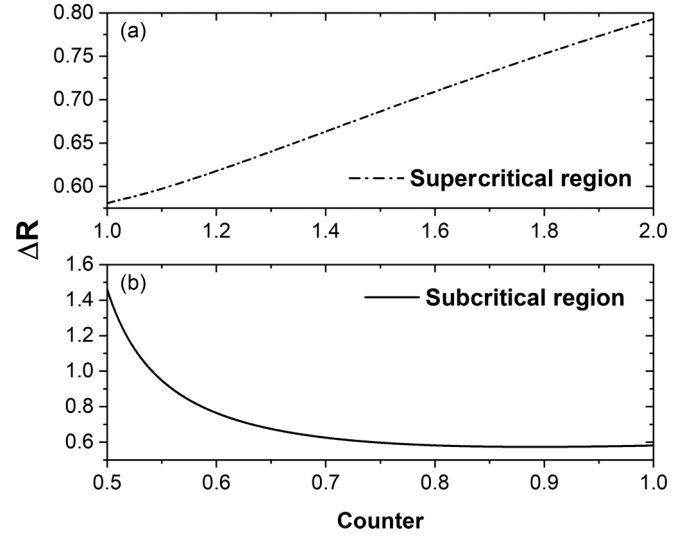


FIG. 7. Normalized difference between classical and semiclassical SW curvatures for $\lambda^* = 1.5$, $\Delta R = (R_Q^* - R_C^*)/R_Q^*$. This difference is given in terms of reduced temperature $T^+ = T/T_{crit}$ and reduced packing fraction $\eta^+ = \eta/\eta_{crit}$. A counter i is used to evaluate point by point the corresponding value of ΔR for each pair of values (η^+, T^+) . Two regions are described for ΔR : (a) the supercritical region, where the interval is [1.001, 2.0], and (b) the subcritical region, where (η^+, T^+) are equally increasing in the interval [0.5, 0.999]. In the subcritical region $\Delta R \rightarrow 0.6$ as parameters reach the critical point, and in the supercritical region this tendency remains.

both scalars, since the semiclassical and classical systems do not exhibit the same behavior in the same region of the thermodynamic equilibrium space, as observed in Fig. 6.

Two different regions are shown separately. (i) In the lower plot, the values of ΔR in the region of subcritical values of (η^+, T^+) are calculated, in the interval [0.5, 0.999], for which both parameters equally increase. In this plot, it can be noticed that $\Delta R \rightarrow 0.6$ as $(\eta^+, T^+) \rightarrow 1$, i.e., as these parameters reach their critical values. (ii) In the upper plot, the corresponding values of ΔR are calculated for supercritical values of (η^+, T^+) , in the interval of [1.001, 2.0]; similarly to the subcritical case, near the critical values of η^+ and T^+ , the difference ΔR remains close to 0.6, slowly increasing as the value of thermodynamic parameters go up to 2.0 times their critical values. Therefore, Fig. 7 shows that in the presented regions, the semiclassical scalar is always greater than its classical counterpart.

An additional comparison of the differences in the geometric properties of the semiclassical and classical SW fluids is also performed via an analysis of the behavior of the R Widom lines for both systems. As mentioned in the Introduction, these lines are defined in the supercritical region as the locus of the maxima for the isotherms of the scalar curvature R ; this line separates a gaslike phase from a liquidlike phase in the supercritical region for the semiclassical and classical SW fluids. This comparison is presented in Fig. 8 in the (λ_B^+, P^+) representation, instead of the usual temperature-pressure one; therefore, the separation of phases is inverted with respect to the usual case. The most relevant feature of these plots is that when semiclassical and classical Widom lines are compared,

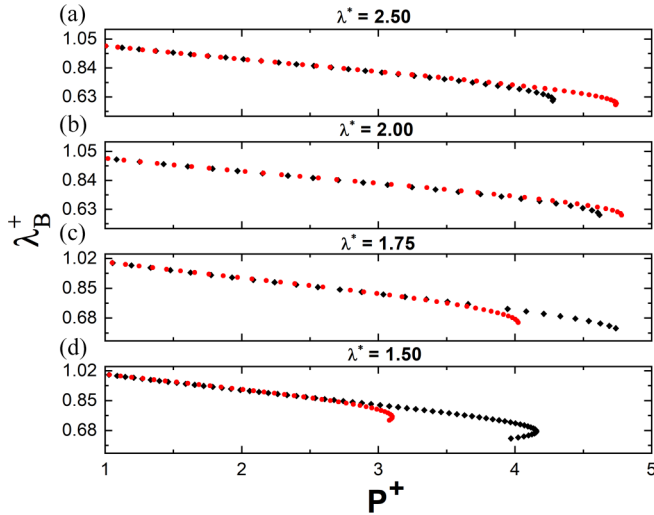


FIG. 8. Comparison of R Widom lines obtained for the semiclassical (circles) and classical (diamonds) SW fluids, given by circles and diamonds, respectively, for the following values of the SW range λ^* : (a) 2.5, (b) 2, (c) 1.75, and (d) 1.5. Results are presented as a function of the reduced de Broglie thermal wavelength $\lambda_B^+ = \lambda_B/\lambda_{B,\text{crit}}$ and the reduced pressure $P^+ = P/P_{\text{crit}}$. In this representation, higher supercritical states are reached as $\lambda_B^+ \rightarrow 0$. Semiclassical and classical lines exhibit the same linear behavior in the region near the critical point. The supercritical line can be extended further for the semiclassical SW fluid for smaller potential ranges. Interestingly, this behavior is reversed as λ^* increases.

these lines are range dependent. For smaller ranges ($\lambda^* < 2.0$), a shorter Widom line is obtained for the semiclassical system. For instance, when $\lambda^* = 1.5$ the semiclassical line cuts around $P^+ \approx 3$, while its classical counterpart has a linear behavior up to $P^+ \approx 4$. This situation is reversed, however, as λ^* is increased, as can be seen for $\lambda^* = 2.0$; in this case the longest Widom line is the semiclassical one. Therefore, for greater values of the SW range, the line that separates the aforementioned liquidlike phase from the gaslike one is more persistent for the semiclassical system. However, in all cases the Widom line ends not far from the critical point, that is, the maximum in the curvature scalar disappears when we move away from the critical point, in a similar way to what happens with the extrema of response functions.

IV. CONCLUSION

In this work we briefly explored the thermodynamic geometry of semiclassical fluids. Two different models were analyzed, a SCHS fluid whose Helmholtz free energy is ob-

tained from PIMC simulations and a semiclassical SSW fluid, described by a semiclassical hard-sphere repulsive interaction coupled with a classical attractive square-well contribution. The curvature obtained from the SCHS potential presents important differences compared to its classical counterpart.

It was found that when quantum contributions are taken into account, the BPH anomaly is partially reversed, in a region in the middle of the plane (λ_B^*, η) where the considered SCHS equation of state is valid. For the regions of low and high densities, R_{SCHS} exhibits the same anomalous behavior as its classical counterpart. It is not surprising that at lower densities the classical anomalous behavior remains; however, it is interesting that at the regime of high densities the SCHS curvature tends to return to the anomalous classical behavior since it resembles the behavior of other semiclassical systems [6].

Regarding the geometric properties of the semiclassical SSW fluid when compared to the classical one, interesting differences were found between both systems. For instance, the critical points for temperature and density of the semiclassical system are significantly lower than the classical ones, which can be noticed in the direct comparison of the supercritical curvatures depicted in Fig. 6. This comparison was further explored for the normalized difference $\Delta R = (R_Q^* - R_C^*)/R_Q^*$, where we found, for each of the cases explored, that the semiclassical curvature is always greater than the classical one. Finally, the supercritical R Widom lines for both systems were also determined and compared, showing that near the critical point both lines practically overlap. Interestingly, it was found that the length of these lines is also potential-range dependent, and the length for ranges below $\lambda^* = 2.0$ is larger for the classical SW fluid, which is reversed for ranges above this value. We were then able to distinguish the liquidlike phase from the gaslike one deeper into the supercritical region when compared to the classical one.

It is clear that this research represents only an initial step in the study of semiclassical fluids within the framework of thermodynamic geometry and more work is needed to clarify the influence and consequences of quantum effects in these systems.

ACKNOWLEDGMENTS

J.T.-A. acknowledges support from Universidad de Guanajuato through Grant No. 042/2024 of Convocatoria Institucional de Investigación Científica. L.F.E.-H. acknowledges support from CONAHCYT (Consejo Nacional de Humanidades Ciencias y Tecnologías) CVU 230753 through the postdoctoral grant Estancias Posdoctorales por México para la Formación y Consolidación de las y los Investigadores por México.

- [1] X.-Z. Li, B. Walker, and A. Michaelides, *Proc. Natl. Acad. Sci. USA* **108**, 6369 (2011).
 [2] S. Contreras, C. Serna, and A. Gil-Villegas, *J. Chem. Eng. Data* **65**, 5933 (2020).
 [3] B.-J. Yoon and H. A. Scheraga, *J. Chem. Phys.* **88**, 3923 (1988).

- [4] K. J. Runge and G. V. Chester, *Phys. Rev. B* **38**, 135 (1988).
 [5] L. M. Sesé, *Mol. Phys.* **74**, 177 (1991).
 [6] T. E. Markland, J. A. Morrone, B. J. Berne, K. Miyazaki, E. Rabani, and D. R. Reichman, *Nat. Phys.* **7**, 134 (2011).
 [7] N. Singh and S. K. Sinha, *J. Chem. Phys.* **69**, 2709 (1978).

- [8] C. Serna and A. Gil-Villegas, *Mol. Phys.* **114**, 2700 (2016).
- [9] B. P. Singh and S. K. Sinha, *Phys. Rev. A* **18**, 2701 (1978).
- [10] J. Barrat, P. Loubeyre, and M. L. Klein, *J. Chem. Phys.* **90**, 5644 (1989).
- [11] B. J. Berne and D. Thirumalai, *Annu. Rev. Phys. Chem.* **37**, 401 (1986).
- [12] D. Chandler and P. G. Wolynes, *J. Chem. Phys.* **74**, 4078 (1981).
- [13] K. Singer and W. Smith, *Mol. Phys.* **64**, 1215 (1988).
- [14] V. M. Trejos and A. Gil-Villegas, *J. Chem. Phys.* **136**, 184506 (2012).
- [15] K. R. Arriola-González, A. Gil-Villegas, and S. Figueroa-Gerstenmaier, *Mol. Phys.* **121**, e2244611 (2023).
- [16] C. R. Rao, *Bull. Calcutta Math. Soc.* **37**, 81 (1945).
- [17] R. Mrugała, *Physica A* **125**, 631 (1984).
- [18] R. Mrugała, J. D. Nulton, J. C. Schön, and P. Salamon, *Phys. Rev. A* **41**, 3156 (1990).
- [19] F. Weinhold, *J. Chem. Phys.* **63**, 2479 (1975).
- [20] G. Ruppeiner, *Phys. Rev. A* **20**, 1608 (1979).
- [21] G. Ruppeiner, *Rev. Mod. Phys.* **67**, 605 (1995).
- [22] P. Salamon, J. Nulton, and E. Ihrig, *J. Chem. Phys.* **80**, 436 (1984).
- [23] M. E. Fisher and B. Widom, *J. Chem. Phys.* **50**, 3756 (1969).
- [24] L. Xu, P. Kumar, S. V. Buldyrev, S.-H. Chen, P. H. Poole, F. Sciortino, and H. E. Stanley, *Proc. Natl. Acad. Sci. USA* **102**, 16558 (2005).
- [25] D. Bolmatov, M. Zhernenkov, D. Zav'yalov, S. N. Tkachev, A. Cunsolo, and Y. Q. Cai, *Sci. Rep.* **5**, 15850 (2015).
- [26] D. Corradini, M. Rovere, and P. Gallo, *J. Chem. Phys.* **143**, 114502 (2015).
- [27] J. Jaramillo-Gutiérrez, J. López-Picón, and J. Torres-Arenas, *J. Mol. Liq.* **347**, 118395 (2022).
- [28] V. V. Brazhkin, Y. D. Fomin, A. G. Lyapin, V. N. Ryzhov, and E. N. Tsiok, *J. Phys. Chem. B* **115**, 14112 (2011).
- [29] I. Zerón, J. Torres-Arenas, E. de Jesús, B. Ramírez, and A. Benavides, *J. Mol. Liq.* **293**, 111518 (2019).
- [30] G. Ruppeiner, *Phys. Rev. E* **86**, 021130 (2012).
- [31] H.-O. May and P. Mausbach, *Phys. Rev. E* **85**, 031201 (2012).
- [32] A. Gil-Villegas, A. Galindo, P. J. Whitehead, S. J. Mills, G. Jackson, and A. N. Burgess, *J. Chem. Phys.* **106**, 4168 (1997).
- [33] B. H. Patel, H. Docherty, S. Varga, A. Galindo, and G. C. Maitland, *Mol. Phys.* **103**, 129 (2005).
- [34] N. F. Carnahan and K. E. Starling, *J. Chem. Phys.* **53**, 600 (1970).
- [35] J. Jaramillo-Gutiérrez, J. López-Picón, and J. Torres-Arenas, *J. Mol. Liq.* **319**, 114213 (2020).
- [36] A. C. Brańka, S. Pieprzyk, and D. M. Heyes, *Phys. Rev. E* **97**, 022119 (2018).
- [37] B. J. Alder, D. A. Young, and M. A. Mark, *J. Chem. Phys.* **56**, 3013 (1972).
- [38] W. R. Smith, D. Henderson, and Y. Tago, *J. Chem. Phys.* **67**, 5308 (1977).
- [39] A. Gil-Villegas, F. del Río, and A. L. Benavides, *Fluid Phase Equilib.* **119**, 97 (1996).
- [40] A. L. Benavides and A. Gil-Villegas, *Mol. Phys.* **97**, 1225 (1999).
- [41] M. Khanpour, *Phys. Rev. E* **83**, 021203 (2011).
- [42] L. Vega, E. de Miguel, L. F. Rull, G. Jackson, and I. A. McLure, *J. Chem. Phys.* **96**, 2296 (1992).
- [43] J. López-Picón, L. Escamilla-Herrera, and J. Torres-Arenas, *J. Mol. Liq.* **368**, 120607 (2022).
- [44] T. Lafitte, A. Apostolakou, C. Avendaño, A. Galindo, C. S. Adjiman, E. A. Müller, and G. Jackson, *J. Chem. Phys.* **139**, 154504 (2013).